Published by Oxford University Press *Human Molecular Genetics, 2002, Vol. 11, No. 21* **2625–2633**

Retention of pendrin in the endoplasmic reticulum is a major mechanism for Pendred syndrome

Pnina Rotman-Pikielny[1,†], Koret Hirschberg[6,†], Padma Maruvada[1], Koichi Suzuki[4], Ines E. Royaux[2], Eric D. Green[2], Leonard D. Kohn[5], Jennifer Lippincott-Schwartz[3] and Paul M. Yen[1,*]

[1]Clinical Endocrinology Branch, NIDDK, [2]Genome Technology Branch, NHGRI, and [3]Cell Biology and Metabolism Branch, NICHD, National Institutes of Health, Bethesda, Maryland 20892, USA, [4]National Institute of Infectious Diseases, Higashimurayama, Tokyo, Japan, [5]Department of Biomedical Sciences and Edison Biotechnology Institute, Ohio University College of Osteopathic Medicine, Athens, Ohio, USA and [6]Department of Pathology, Sackler School of Medicine, Tel Aviv University, Tel Aviv, Israel

Received June 7, 2002; Revised and Accepted July 27, 2002

Pendred syndrome is a major cause of congenital deafness, goiter and defective iodide organification. Mutations in the transmembrane protein, pendrin, cause diminished export of iodide from thyroid follicular cells to the colloid and are associated with the syndrome. We used green fluorescent protein (GFP) chimeras of wild-type (WT) pendrin and three common natural mutants (L236P, T416P and G384) to study their intracellular trafficking in living cells. Time-lapse imaging, dual color labeling and fluorescent recovery after photobleaching (FRAP) studies demonstrated that GFP–WT pendrin targets to the plasma membrane. In contrast, all three mutant pendrins were retained in the endoplasmic reticulum (ER) in co-localization studies with ER and Golgi markers. The ER retention of L236P appeared to be selective as this mutant did not prevent a viral membrane protein, VSVGtsO45 or wild-type pendrin from targeting the plasma membrane. These findings suggest that ER retention and defective plasma membrane targeting of pendrin mutants play a key role in the pathogenesis of Pendred syndrome.

INTRODUCTION

Pendred syndrome is an autosomal recessive disorder characterized by congenital deafness, goiter and defective iodide organification (1). The Pendred gene, *PDS*, is a member of the SLC26A gene family (2). The gene product, pendrin, is a 73 kDa glycoprotein which contains 11 or 12 transmembrane domains and is an iodide chloride transporter that resides in the apical pole of thyroid follicular cells (3,4). Iodide is transported from the bloodstream into follicular cells by the sodium iodide symporter (NIS) located on the basolateral surface, and then is delivered to the colloid reservoir via pendrin. This efficient iodide-trapping mechanism leads to oxidation and organification of iodide on tyrosine residues of thyroglobulin macromolecules which, in turn, are enzymatically coupled to form thyroid hormones (triiodithyronine, T_3; thyroxine, T_4). Patients with Pendred syndrome have an organification defect in thyroid hormone synthesis and typically have abnormal perchlorate discharge tests (5).

More than 35 different pendrin mutations have been identified so far in the *PDS* gene, which typically result in amino acid substitutions or frame shift mutations scattered throughout the protein (6). These, in turn, cause either classical Pendred syndrome or non-syndromic deafness. The most common mutations, L236P and T416P, account for more than 50% of cases of Pendred syndrome (7). Recently, it has been shown that several natural mutants have decreased iodide and chloride transport when their cRNAs were injected into Xenopus oocytes (8). The mechanism(s) underlying the functional defects of the mutant pendrins is not known.

Recently, several genetic diseases have been associated with defective membrane trafficking (9). For example, in cystic fibrosis, mutations in the transmembrane conductance regulator cause aberrant folding, resulting in its retention in the

*To whom correspondence should be addressed at: Molecular Regulation and Neuroendocrinology Section, Clinical Endocrinology Branch, National Institutes of Health, Building 10, Room 8D12, Bethesda, Maryland 20892; Tel: +1 3015946797; Fax: +1 3014024136; Email: pauly@intra.niddk.nih.gov

†The authors wish it to be known that, in their opinion, the first two authors should be treated as joint First Authors.

endoplasmic reticulum (ER) and degradation by the ubiquitin proteasome pathway (10,11). In α1-antitrypsin deficiency, mutations in α1-antitrypsin cause its retention in the ER and prevent its secretion into the blood stream, resulting in hepatitis and emphysema. Additionally, in more than 70% of cases of nephrogenic diabetes insipidus (NDI), mutations in the vasopressin V_2 receptor prevent it from reaching the plasma membrane (PM) (12).

In order to study whether defective membrane trafficking may be involved in the pathogenesis of Pendred syndrome, we used green fluorescent protein (GFP) technology to investigate the intracellular distribution and trafficking of wild type (WT) and three natural mutant pendrins in living cells. Time-lapse imaging, dual color labeling and fluorescence recovery after photobleaching (FRAP) studies demonstrated that GFP–WT pendrin correctly targets to the plasma membrane (PM), whereas the GFP-tagged mutant pendrins are retained in the ER. We propose that defective PM targeting of mutant pendrins plays a key role in the pathogenesis of Pendred syndrome and provides new insight into cellular trafficking and disease.

RESULTS

GFP-pendrin targets to the plasma membrane

COS7 cells were transiently transfected with GFP–WT pendrin expressing vector and visualized by confocal laser scanning microscopy (CLSM) after overnight incubation at 37°C. At steady state, GFP–WT pendrin was observed predominantly in the plasma membrane (PM) with a small pool of the protein present in the ER (Fig. 1A). Thus, GFP-tagging did not inhibit the targeting of pendrin to the PM. The ER resident population likely represented a newly synthesized pool of GFP–WT pendrin since cycloheximide treatment prior to imaging diminished this population (data not shown). GFP–WT pendrin was then expressed in FRTL5 cells, a rat thyroid cell-line expressing endogenous pendrin (3) and also found to be predominantly located in the PM as observed in the 90° (z plane) projection (Fig. 1B). However, unlike COS7 cells with their significant ER distribution, most FRTL5 cells had a significant pool of GFP–WT pendrin in the Golgi complex. ER and Golgi localizations were confirmed with anti-COP1 and anti-calreticulin antibodies (Golgi and ER markers, respectively) (data not shown). Indirect immunofluorescence labeling using anti-pendrin antibody showed a similar distribution pattern for endogenous pendrin and GFP–WT pendrin in FRTL5 cells, further confirming the correct targeting of GFP–WT pendrin (data not shown). PM targeting of GFP–WT pendrin was observed also in MDCK and CV1 cells (data not shown).

To verify the Golgi pool of GFP–WT pendrin in FRTL5 cells is delivered to the PM rather than irreversibly retained in the Golgi complex (12) we used selective photobleaching of the PM of transfected FRTL5 cells to detect the movement of GFP–WT pendrin via transport intermediates from the unbleached Golgi to the PM (Fig. 1C, third panel insert). Reappearance of GFP–WT pendrin at the PM was seen less than a minute after photobleaching and complete recovery occurred by ∼7 minutes (Fig. 1C, third and fourth panels). Thus, intracellular transport of GFP–WT pendrin can be visualized along the entire secretory pathway. As an additional control, yellow fluorescent protein (YFP)–WT pendrin and a temperature-sensitive PM protein, VSVGtsO45 cyan fluorescent protein (CFP) (CFP–VSVG) (13), co-localized in the ruffles of the PM (Fig. 1D).

L236P, T416P and G384E are retained in the ER

The intracellular distribution of the pendrin mutant, L236P (amino acid substitution located in the fourth transmembrane domain), was studied by indirect immunofluorescence with anti-human pendrin antibody (14). Surprisingly, we observed that L236P was completely retained in the ER in transfected COS7 cells, seen as an elaborate reticulum extending off the nuclear envelope (Fig. 2A, left panel). In order to further study the distribution of this and two other common pendrin mutants in living cells, COS7 cells were transfected with vectors encoding GFP chimeras with pendrin mutants L236P, T416P, or G384E (amino acid substitutions for latter mutants located in the eight transmembrane domain and the fourth intracellular loop, respectively). All three GFP-tagged mutants consistently localized within the ER (Fig. 2B). Furthermore, ER retention of the most common mutant, GFP-tagged L236P was demonstrated in FRTL5 cells (Fig. 2A, right panel). Similar data were obtained in CV1 (Fig. 3A) and MDCK cell-lines (data not shown).

Indirect immunofluorescence experiments with anti-calreticulin (ER marker) antibody confirmed that GFP–L236P is located within ER membranes (Fig. 3A upper panel). Additionally, GFP–L236P did not co-localize with the Golgi marker, COPI, stained with anti-COPI antibody (data not shown). In many transfected cells, a high level of fluorescence was detected in the juxtanuclear region (Figs 2B and 3B, right panel arrowheads), which could be due to accumulation of mutant pendrin deforming the normal ER membrane architecture. Therefore, as an additional control, L236P tagged to the yellow fluorescent variant of GFP and a Golgi marker, galactosyltransferase (GalT), tagged to the cyan fluorescent variant of GFP were co-expressed in COS7 cells. Figure 3B demonstrates that the condensed juxtanuclear L236P (right panel arrowheads) does not co-localize with GalT in the Golgi complex. Additionally, when living cells co-expressing YFP–L236P and CFP–GalT were incubated for several hours at 20°C (a temperature that causes accumulation of cargo in the Golgi complex (15)), no mutant pendrin was seen in the Golgi (data not shown).

Diffusion of L236P within ER membranes

The inability of the transport machinery to export the mutant proteins causes ER retention. This could either be due to improper protein folding or elimination of an essential targeting signal (16) causing immobilization and aggregation of the mutant protein in the ER membranes. To study the behavior of L236P within the ER, we analyzed the diffusion of GFP–L236P within ER membranes using fluorescence recovery after photobleaching (FRAP) (Fig. 4) (13). A rectangular ER region was photobleached and images were collected to monitor the lateral diffusion of GFP–L236P into the photobleached region. Full recovery was observed by ∼150 seconds,

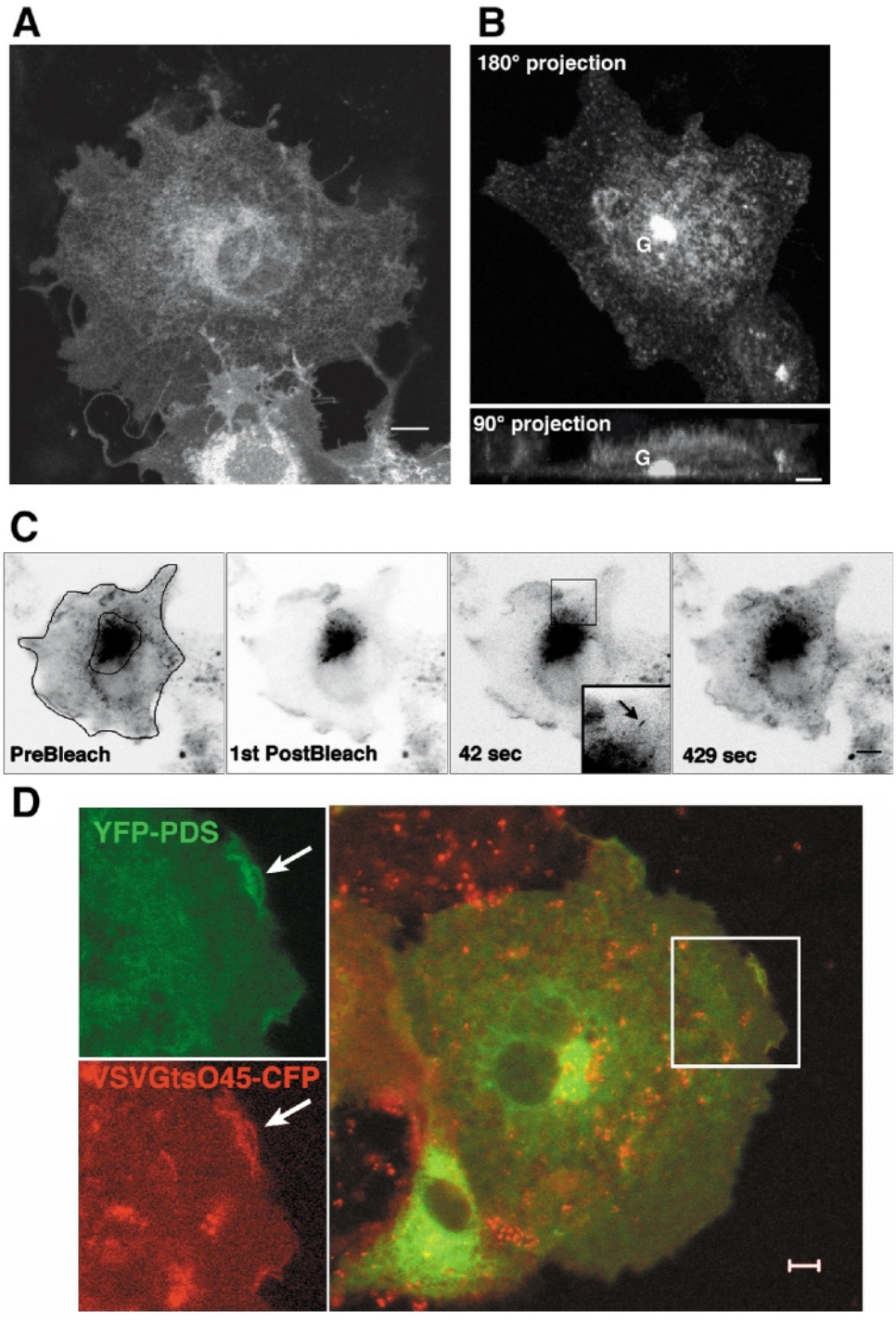

Figure 1. Intracellular localization and trafficking of GFP–WT pendrin. Confocal images of GFP–WT pendrin in COS7 (**A**) and FRTL5 (**B** and **C**) cells. Cells were transiently transfected with a GFP–pendrin encoding vector and visualized after overnight incubation at 37°C as described in Materials and Methods. The 180° (xy plane) and 90° (z plane) projections of a FRTL5 cell expressing GFP–WT pendrin (B) were reconstructed from 40 confocal images. The intense central spot represents the Golgi (G). To visualize Golgi to PM trafficking of GFP–WT pendrin (C), a region of interest excluding the Golgi was continuously photobleached and post-bleach images were collected at 3 second intervals. Images are inverted to demonstrate the increase in PM fluorescence after bleach. Inset at the 42 second time point indicates a Golgi to PM tubular transport intermediate containing GFP–pendrin (**D**) Right panel. Confocal image of a living COS7 cell expressing YFP–WT pendrin (green) with CFP–VSVGtsO45 (red) incubated for 20 hours at the permissive temperature (32°C) for CFP–VSVGtsO45 to localize at the PM. Left panels. Enlarged images (2×) of insert in right panel, showing YFP–WT pendrin and CFP–VSVGtsO45 co-expression at the plasma membrane. Arrows point to PM membrane ruffles where both proteins are co-expressed. Scale bars represent 5 μm.

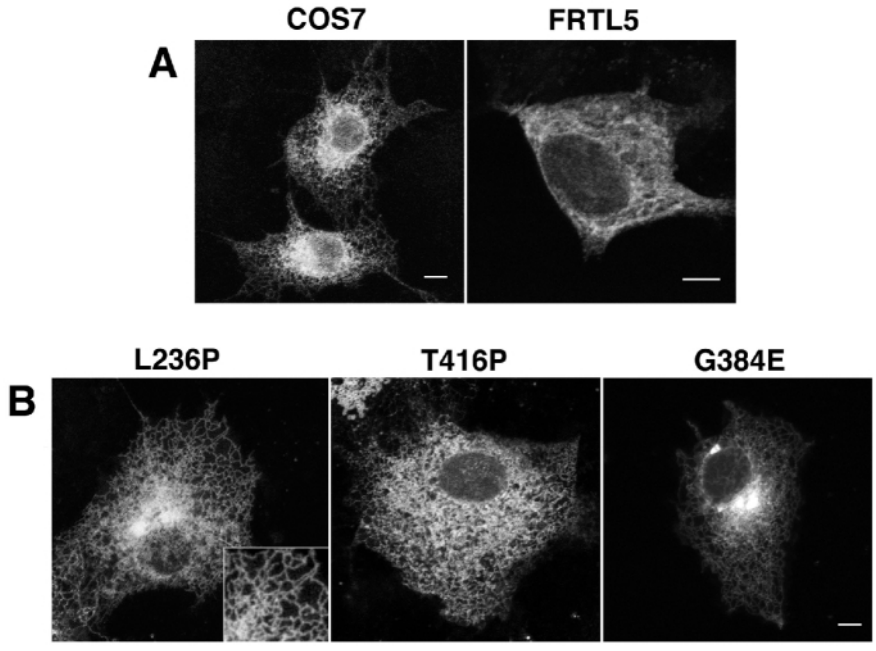

Figure 2. Intracellular localization of pendrin mutants. (**A**) Confocal images showing indirect immunofluorescent staining of untagged L236P in COS7 cells (left panel) and of GFP–L236P in a living FRTL5 cell (right panel). COS7 cells were fixed 16 hours after transfection and stained with anti-human pendrin antibody (13). FRTL5 cells were transfected and visualized as described in the Materials and Methods section. (**B**) Confocal images of living COS7 cells transiently transfected with vectors encoding GFP-tagged L236P, T416P and G384E pendrin mutants (left, center and right panels respectively). Scale bars represent 5 μm.

with no apparent immobile fraction; thus, L236P does not aggregate within ER membranes. Also supporting this point is the observation that L236P was evenly distributed throughout the entire ER without any gross evidence for aggregation (Figs 2 and 3).

The effective diffusion coefficient was determined by using the previously described ER diffusion simulation protocol (17), and found to be $\sim D_{app} = 0.04\ \mu m^2/sec$ for GFP–L236P in ER membranes. This diffusion coefficient represents the rate in which unbleached GFP–L236P exchanges with the bleached protein in the photobleached area. The ER diffusion co-efficient for L236P was ~1/10 of that determined for several other GFP fusion proteins known to reside in the ER such as lamin-B receptor, β subunit of the signal-recognition-particle receptor and Golgi enzyme galactosyltransferase (13).

Effect of L236P on general ER trafficking

The retention of GFP–L236P in the ER could be specific or have a general effect on ER function as misfolded protein could prevent the exit of other cargo proteins from the ER (18). To test this latter possibility, YFP–L236P was co-expressed with the CFP fusion of the viral glycoprotein, VSVGtsO45 (CFP–VSVG) (19). VSVGtsO45 is a membranous protein that reversibly misfolds in the ER at non-permissive temperatures (above 39.5°C), and consequently is not recognized by the ER export machinery (13). Upon temperature shift to 32°C, VSVGtsO45 refolds correctly and moves as a synchronous population to the Golgi complex before being transported to the PM. Since these properties are preserved in the GFP-tagged protein, it has been used extensively to study intracellular transport along the secretory pathway (13,20,21). When transfected cells were incubated at 40°C, both GFP–L236P and CFP–VSVG accumulated in the ER (data not shown). However, upon shift to a permissive temperature (32°C), CFP–VSVG was transported efficiently to the PM (Fig. 5B). In contrast, YFP–L236P did not change its cellular distribution (Fig. 5A). The merged image (Fig. 5C) depicts the cellular distribution of both protein constructs 50 minutes after temperature shift to the permissive temperature. These results are noteworthy since YFP–L236P was unable to exit the ER despite a massive efflux of CFP–VSVG from the ER upon temperature shift to the permissive temperature.

Effect of L236P on WT pendrin trafficking

Since Pendred syndrome is an autosomal recessive disorder requiring two mutant Pendred alleles, we examined the effect of mutant pendrin on ER efflux of WT pendrin by co-expressing CFP–WT pendrin with YFP–L236P in COS7 cells. Although a significant pool remained in the ER, CFP–WT pendrin correctly targeted to the PM (Fig. 6B and 6C). In contrast, YFP–L236P remained exclusively in the ER (Fig. 6A). Thus, retention of L236P in the ER did not prevent the egress and PM targeting of either the viral protein marker, VSVGtsO45, or WT pendrin.

DISCUSSION

Although Pendred syndrome was first described over 100 years ago, the molecular mechanism for cellular defects in the thyroid and cochlea has not been described previously.

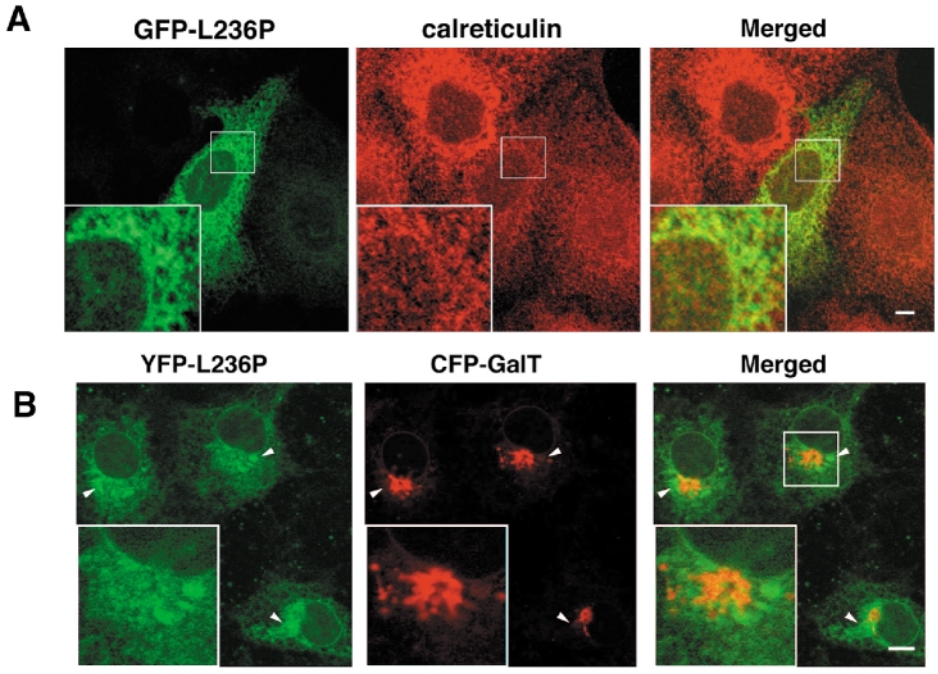

Figure 3. Determination of intracellular localization of GFP–L236P by co-localization studies. (**A**) Confocal images of fixed CV1 cells transiently expressing GFP–L236P (left panel) and immunofluorescent staining with anti-calreticulin antibodies (middle panel). The merged image (right panel) indicates that both proteins colocalize within ER membranes (yellow color). Inserts show enlarged images (2×) of ER membranes. (**B**) Confocal image of living COS7 cells co-expressing YFP–L236P (left panel) together with the CFP–tagged Golgi marker, GalT (middle panel). The merged image (right panel) shows that YFP–L236P is completely segregated from the Golgi complex. Arrowheads (at lower merged panel) point to juxtanuclear pools of YFP–L236P which do not colocalize with the Golgi. Scale bars represent 5 μm.

Recently, mutations in the iodide chloride transporter, pendrin, have been shown to be associated with Pendred syndrome and non-syndromic deafness. Here we show that three common natural pendrin mutants, which account for more than 50% of the cases of this syndrome, are retained in the ER and do not reach the PM. Thus, we have characterized the major cellular mechanism by which mutations in pendrin cause Pendred syndrome.

Our studies showed that GFP–WT pendrin is efficiently targeted to the cell membrane in several cell lines, including FRTL5 thyroid cells that endogenously express pendrin. Although the steady state intracellular distribution of GFP–WT pendrin was different in COS7 and FRTL5 cells, the protein was predominantly expressed on the PM in both cell lines. The localization of GFP–WT pendrin in the ER of COS7 cells and in the Golgi complex of FRTL5 cells, respectively, may be due to differences in protein folding or trafficking rates along the secretory pathway in these two cell lines. Additionally, the ER pool in COS7 cells could be chased-out with the protein synthesis inhibitor, cycloheximide (Hirschberg and Rotman-Pikielny, unpublished results), and the Golgi pool in FRTL5 cells could exit and target the PM in photobleaching experiments (Fig. 1C).

We also showed that three natural pendrin mutants are retained in the ER using GFP-chimeras. Mutations scattered throughout the pendrin gene can cause either Pendred syndrome or non-syndromic deafness; however only two mutations have been found in common in families with either condition (7,22). Patients with our particular mutant pendrins displayed classical Pendred syndrome. Additionally, detailed studies of GFP–L236P, which contains the most common pendrin mutation, showed ER retention by co-localization with a specific ER marker, calreticulin, and by lack of co-localization with the Golgi markers, CFP–GalT or COP-1. The ER retention of untagged L236P in FRTL5 cells was further confirmed by indirect immunofluorescence studies with anti-pendrin antibody. Interestingly, L236P retention in the ER did not prevent two other proteins, VSVGtsO45 or WT pendrin, from correctly targeting the PM. These findings suggest that ER retention of L236P was selective. Moreover, the inability of this mutant pendrin to prevent the arrival of WT pendrin at the plasma membrane is consistent with the clinical observation that Pendred syndrome is an autosomal recessive disorder in which heterozygous patients are unaffected. Thus, partial expression of pendrin transporters on the PM of thyroid cells may be sufficient for a normal phenotype. Recently, it was shown that homozygous *PDS* knockout mice (−/−) have marked loss of hearing without thyroid manifestations, suggesting that the ear may be more sensitive to pendrin loss (23), and raising the possibility of an alternative iodine transporter(s) in the murine thyroid gland.

We also showed that although GFP–L236P could not be transported to the Golgi complex, it still could diffuse freely within the ER, albeit at a slower rate than most other proteins within the ER (13). Recently, a variety of reagents such as glycerol, dimethylsulfoxide or trimethylamine-N-oxide have been used to rescue mutant cystic fibrosis transmembrane conductance regulator proteins from the ER and allow their

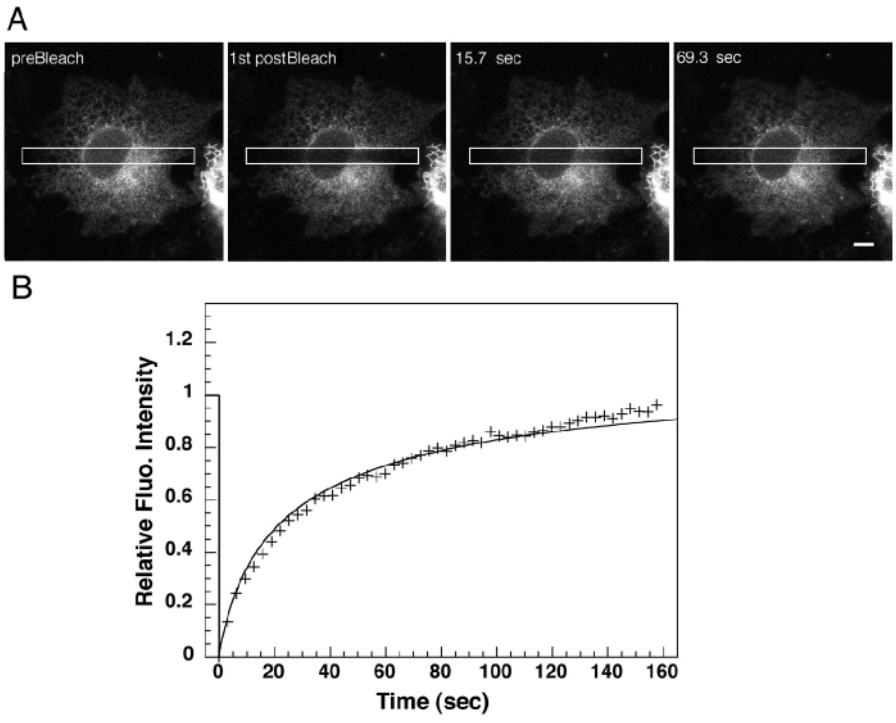

Figure 4. FRAP analysis of GFP–L236P in the ER membranes (**A**) FRAP analysis of cells transiently transfected with GFP–L236P encoding vector. COS7 cells were transfected and visualized as in Figure 1. Images were obtained before photobleaching and at 3 second intervals thereafter as described in Materials and Methods. The photobleached area is outlined by a box. Scale bars represent 5 μm. (**B**) The extent and time course of recovery after photobleaching of L236P as measured by the average fluorescence intensity within the bleachbox (+ curve) compared to the simulated data for diffusion within the ER (straight line curve). Detailed description is available in Materials and Methods.

targeting to the cell membrane with partial restoration of their function (24,25). These pharmacological chaperones thus have the potential for renaturing trapped mutant proteins *in vivo*, and promoting their normal targeting and function. Patients with Pendred syndrome as well as those with other diseases which have proteins trapped in the ER could potentially benefit from such a pharmacological strategy. In this connection, it is interesting to note that the putative ion transport region of pendrin is located in the second transmembrane domain which is amino-terminal to the mutation sites of the pendrin mutants studied (2).

In summary, our studies show that, in contrast to WT pendrin which is targeted to the PM, three common pendrin mutants that account for over 50% of affected patients with Pendred syndrome are retained in the ER. These real-time imaging studies were conducted in living cells using time-lapse imaging, dual fluorescent labeling and FRAP analyses. In this connection and concurrent with our studies, Taylor *et al.* recently have identified several mutant pendrins, including L236P, that also are retained in the ER and exhibit decreased iodide transport (26). Additionally, our findings show that L236P does not aggregate within the ER but has a slow diffusion rate. Furthermore, it does not block egress of either WT pendrin or another plasma membrane proteins such as VSVGtsO45 and thus may explain the lack of phenotype in heterozygote family members carrying the mutant *PDS* gene. Although it is possible that some other pendrin mutants may be functionally impaired despite targeting to the PM, or frame-shift mutants could be poorly expressed in the cell, our findings nonetheless show that defective PM targeting of pendrin is the major cellular cause of this syndrome in the majority of patients with Pendred syndrome. Since this syndrome is associated with thyroid malfunction and hearing deficits, our findings also provide an important step in understanding how mutations in this protein can cause disease in two diverse organs. The intracellular trafficking of WT and mutant pendrins also may serve as a model for the study and treatment of a growing number of diseases which have defective targeting to the PM or secretion due to protein misfolding.

MATERIALS AND METHODS

Cell culture and expression of GFP chimeras

All cells were grown at 37°C in a humidified atmosphere with 5% CO_2. COS7 (African green monkey cells) were obtained and grown as described previously. Cell cultures were maintained in Dulbecco's modified Eagle's medium (DMEM) (Biofluids, Rockville, MD, USA) supplemented with 10% fetal bovine serum (FBS) and penicillin/streptomycin. For microscopy, cells were subcultured into glass coverslip chambers (Nalg Nunc Int., Naperville, IL, USA). Cells were grown to 50–60% confluence and then transfected with 1.5 μg DNA/

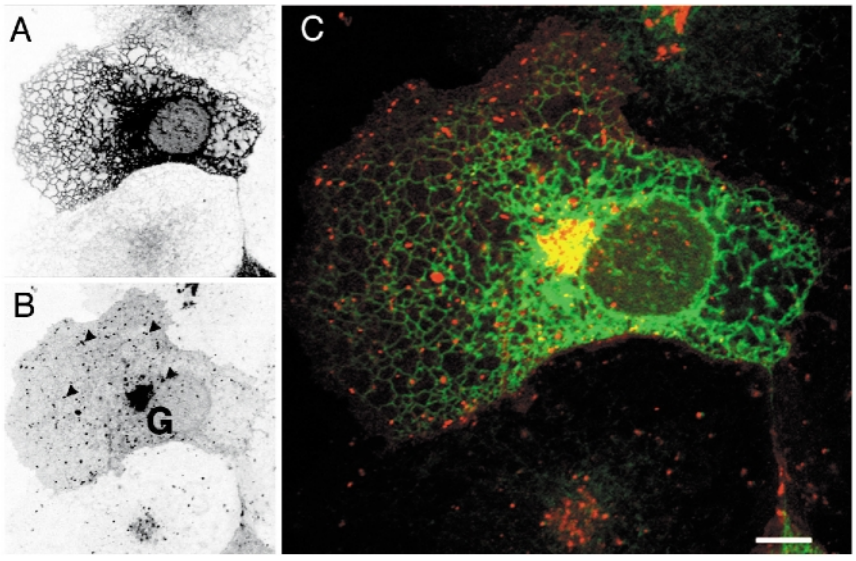

Figure 5. GFP–L236P retention in the ER and its effect on protein export from ER. Confocal image of a living COS7 cell co-expressing YFP–L236P (**A**) with VSVGtsO45–CFP (**B**) incubated for 50 minutes at permissive temperature (32°C), after an overnight pre-incubation at non-permissive temperature (39.5°C). COS7 cells were transfected and visualized as in Figure 1. In contrast to YFP–L236P which localizes to the ER (A), VSVGtsO45–CFP was transported to the Golgi (G) and then to the PM via transport intermediates (arrowheads) (B). A merged image of YFP–L236P and VSVGtsO45–CFP is shown in **C**. Scale bars represent 5 μm.

chamber using FuGENE6 reagent (Roche Molecular Biochemicals, Indianapolis, IN, USA). CLSM images were taken ∼16 hours after transfection.

The rat thyroid cell line, FRTL5, was grown in Coon's modified Ham's f-12 medium supplemented with 5% calf serum (Life Technologies, Inc./BRL, Gaithersburg, MD, USA) and a six-hormone mixture (6H medium), containing bovine TSH (1×10^{-10} M), insulin (10 μg/ml), cortisol (0.4 ng/ml), transferrin (5 μg/ml, glycyl-L-histidyl-L-lysin acetate (10 ng/ml) and somatostatin (10 ng/ml). Medium was changed every three days and cells were passaged every 6–8 days. FRTL5 cells were transfected by electroporation. Electroporation was carried out in 400 μl DMEM containing 20 mM PIPES pH = 7.0, 128 mM glutamate, 10 μm Ca acetate, 2 mM Mg acetate using 800 μF capacitance and 400 V.

For indirect immunofluorescent assays, cells were fixed with 2% formaldehyde, permeabilzed with 0.2% saponin and stained with anti-human pendrin 766–780, anti-COP-1, and anti-reticulin antibodies (14,21,27).

Constructs

PDS cDNA fragment was generated by PCR from full length human *PDS* cDNA in a pcDNA3.1(−)mycHis expression vector (Invitrogen, San Diego, CA, USA) (4). The following primers were used: 5′ primer: TATC**CTCGAG**ATATGGCAG-CGCCAGGCGGCAGGTCG and 3′ primer: GCCCGC**GGTA-CC**TCAGGATGCAAGTGTACGCATAGC containing *Xho*I and *Kpn*I sites, respectively. The *PDS* cDNA fragment was purified, digested with the *Xho*I and *Kpn*I restriction enzymes and subcloned into various GFP expression vectors, pEGFP-C1, pECFP-C1 or pEYFP-C1 (Clontech, Palo Alto, CA, USA), downstream to the fluorescent-protein encoding fragment. Construct sequences were then verified.

L236P mutant was created by a PCR reaction, using a 5′ primer that contained the mutation along with a unique restriction site and the original 3′ primer. The primer sequences were: 5′ primer: GCTGCCTT**CCAAGTGCTGG**TCTCACA-GCC∗AAAGATTGTCCTCAAT (*Pfl*MI site is bolded, mutation is highlighted with ∗). PCR fragment was purified, digested with *Pfl*MI and *Kpn*I and subcloned into a GFP–hPDS vector that was previously digested with the same restriction enzymes. pEBFP–L236P and pECFP–L236P plasmids were created by digesting the full-length L236P mutant with *Xho*I and *Kpn*I and subcloning it to the new vector using the same restriction enzymes.

T416P and E384G *PDS* mutations were constructed using the QuickChange™ Site-Directed Mutagenesis Kit (Stratagene, La Jolla, CA, USA) according to the manufacturer's instructions. Briefly, for each mutation, two complementary HPLC purified primers were synthesized which contained the desired point mutation flanked by unmodified nucleotide sequence.

T416P primers: 5′ primer: GCCGTCCAGGAGAGCCCTG-GAGGAAAGACACAG and 3′ primer: CTGTGTCTTTCCA-GGGCTCTCCTGGACGGC. E384G primers: 5′ primer: GAT-GGGAACCAGGGATTCATTGCCTTTGGGATC and 3′ primer: GATCCCAAAGGCAATGAATCCCTGGTTCCC-ATC. PCR was performed using *Pfu* Turbo DNA polymerase on a GFP–*PDS* plasmid template, resulting in nicked circular strands that contained the desired mutation. The methylated, nonmutated parental strand was then digested with *Dpn*I for 1–3 hours and transformed into XL1-Blue supercompetent cells using a standard heat-shock protocol. During transformation in these cells, nicks in the mutated plasmids were repaired. Colonies containing plasmids then were selected using a blue/white color screen on antibiotic plates containing IPTG and β-gal. Plasmid DNA was extracted from overnight cultures of individual colonies and checked for the desired mutations by direct sequencing.

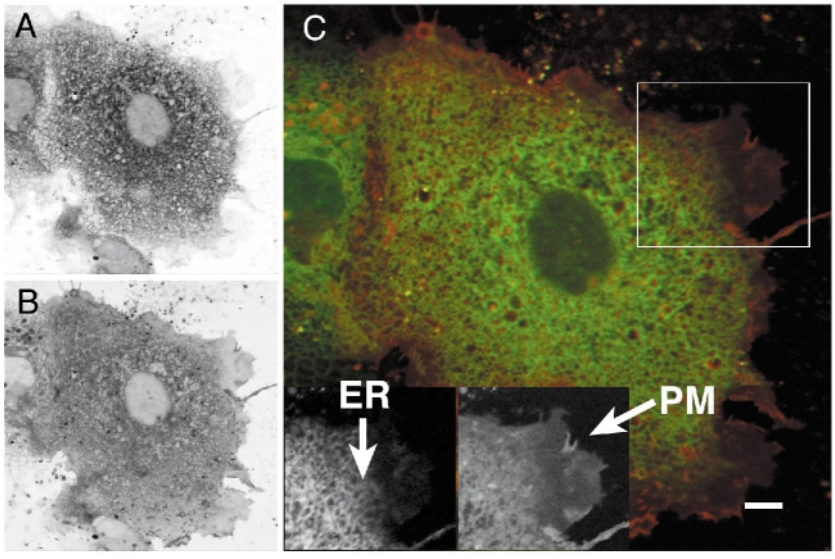

Figure 6. Effect of YFP–L236P on CFP–WT pendrin transport from ER to PM. Confocal image of a living COS7 cell co-expressing YFP–L236P (**A**) with CFP–WT (**B**) pendrin. COS7 cells were transfected and visualized as in Figure 1. YFP–L236P is retained in the ER (A) whereas CFP–WT pendrin was targeted to the PM (B). Merged image of both is shown in **C**. Scale bars represent 5 µm.

Microscopy

Fluorescence images were obtained with a Zeiss LSM 510 or Zeiss LSM 410 confocal microscope using 413 nm laser excitation for CFP, 488 nm for GFP or fluorescein, 514 nm for YFP and 543 nm for rhodamine. Filter sets were as supplied by the manufacturer. Live cells were visualized at 37°C on the microscope stage. Images were captured with either 63 × 1.4 NA or 100 × 1.4 NA objective using a pinhole diameter equivalent to one to two Airey units. Selective photobleaching was carried out using 3–5 consecutive scans of the appropriate laser line at full power and recovery was then monitored by time-lapse imaging at low intensity illumination. Images were analyzed using the Zeiss LSM software or NIH Image software (W. Rasband, NIH, Bethesda, MD, USA).

FRAP analyses

Analysis was performed on a temperature-controlled stage of a Zeiss LSM 510 confocal microscope, using the 488 nm line of a 40 mW Ar/Kr laser with a 63 × 1.4 NA objective. A defined region, 4–5 µm-wide strip extending across cell borders (outlined box in Fig. 4) was photobleached at full laser power (100% power, 100% transmission); recovery of fluorescence was monitored by scanning the whole cell at low laser power. No photobleaching was observed during recovery. Quantitative analysis was performed using the simulation program as described previously (17), where the effective diffusion coefficient is calculated using a simulation algorithm that takes into account the fact that the ER membranes are a complex reticular surface.

ACKNOWLEDGEMENTS

We thank Drs Lawrence P. Karniski and V.C. Sheffield (University of Iowa, IA, USA) for their advice in generating pendrin mutants. We also thank Dr Ann Kenworthy (NICHD, NIH, Bethesda, MD, USA) for her advice in the lateral diffusion analysis of the pendrin mutant.

REFERENCES

1. Kopp, P. (2000) Pendred's syndrome and genetic defects in thyroid hormone synthesis. *Rev. Endocr. Metab. Disord.*, **1**, 109–121.
2. Everett, L.A., Glaser, B., Beck, J.C., Idol, J.R., Buchs, A., Heyman, M., Adawi, F., Hazani, E., Nassir, E., Baxevanis, A.D. *et al.* (1997) Pendred syndrome is caused by mutations in a putative sulphate transporter gene (PDS). *Nat. Genet.*, **17**, 411–422.
3. Scott, D.A. and Karniski, L.P. (2000) Human pendrin expressed in Xenopus laevis oocytes mediates chloride/formate exchange. *Am. J. Physiol. Cell. Physiol.*, **278**, C207–C211.
4. Royaux, I.E., Suzuki, K., Mori, A., Katoh, R., Everett, L.A., Kohn, L.D. and Green, E.D. (2000) Pendrin, the protein encoded by the Pendred syndrome gene (*PDS*), is an apical porter of iodide in the thyroid and is regulated by thyroglobulin in FRTL-5 cells. *Endocrinology*, **141**, 839–845.
5. Reardon, W., Coffey, R., Chowdhury, T., Grossman, A., Jan, H., Britton, K., Kendall-Taylor, P. and Trembath, R. (1999) Prevalence, age of onset, and natural history of thyroid disease in Pendred syndrome. *J. Med. Genet.*, **36**, 595–598.
6. Fugazzola, L., Mannavola, D., Cerutti, N., Maghnie, M., Pagella, F., Bianchi, P., Weber, G., Persani, L. and Beck-Peccoz, P. (2000) Molecular analysis of the Pendred's syndrome gene and magnetic resonance imaging studies of the inner ear are essential for the diagnosis of true Pendred's syndrome. *J. Clin. Endocrinol. Metab.*, **85**, 2469–2475.
7. Van Hauwe, P., Everett, L.A., Coucke, P., Scott, D.A., Kraft, M.L., Ris-Stalpers, C., Bolder, C., Otten, B., de Vijider, J.J., Dietrich, N.L. *et al.* (1998) Two frequent missense mutations in Pendred syndrome. *Hum. Mol. Genet.*, **7**, 1099–1104.
8. Scott, D.A., Wang, R., Kreman, T.M., Andrews, M., McDonald, J.M., Bishop, J.R., Smith, R.J., Karniski, L.P. and Sheffield, V.C. (2000)

Functional differences of the PDS gene product are associated with phenotypic variation in patients with Pendred syndrome and non-syndromic hearing loss (DFNB4). *Hum. Mol. Genet.*, **9**, 1709–1715.
9. Kim, P.S. and Arvan, P. (1998) Endocrinopathies in the family of endoplasmic reticulum (ER) storage diseases: disorders of protein trafficking and the role of ER molecular chaperones. *Endocr. Rev.*, **19**, 173–202.
10. Cheng, S.H., Gregory, R.J., Marshall, J., Paul, S., Souza, D.W., White, G.A., O'Riordan, C.R. and Smith, A.E. (1990) Defective intracellular transport and processing of CFTR is the molecular basis of most cystic fibrosis. *Cell*, **63**, 827–834.
11. Jensen, T.J., Loo, M.A., Pind, S., Williams, D.B., Goldberg, A.L. and Riordan, J.R. (1995) Multiple proteolytic systems, including the proteasome, contribute to CFTR processing. *Cell*, **83**, 129–135.
12. Tamarappoo, B.K. and Verkman, A.S. (1998) Defective aquaporin-2 trafficking in nephrogenic diabetes insipidus and correction by chemical chaperones. *J. Clin. Invest.*, **101**, 2257–2267.
13. Nehls, S., Snapp, E.L., Cole, N.B., Zaal, K.J., Kenworthy, A.K., Roberts, T.H., Ellenberg, J., Presley, J.F., Siggia, E. and Lippincott-Schwartz, J. (2000) Dynamics and retention of misfolded proteins in native ER membranes. *Nat. Cell Biol.*, **2**, 288–295.
14. Royaux, I.E., Wall, S.M., Karniski, L.P., Everett, L.A., Suzuki, K., Knepper, M.A. and Green, E.D. (2001) Pendrin, encoded by the Pendred syndrome gene, resides in the apical region of renal intercalated cells and mediates bicarbonate secretion. *Proc. Natl Acad. Sci. USA*, **98**, 4221–4226.
15. Griffiths, G. and Simons, K. (1986) The trans Golgi network: sorting at the exit site of the Golgi complex. *Science*, **234**, 438–443.
16. Nishimura, N., Bannykh, S., Slabough, S., Matteson, J., Altschuler, Y., Hahn, K. and Balch, W.E. (1999) A di-acidic (DXE) code directs concentration of cargo during export from the endoplasmic reticulum. *J. Biol. Chem.*, **274**, 15937–15946.
17. Siggia, E.D., Lippincott-Schwartz, J. and Bekiranov, S. (2000) Diffusion in inhomogeneous media: theory and simulations applied to whole cell photobleach recovery. *Biophys. J.*, **79**, 1761–1770.
18. Hendershot, L.M., Wei, J.Y., Gaut, J.R., Lawson, B., Freiden, P.J. and Murti, K.G. (1995) *In vivo* expression of mammalian BiP ATPase mutants causes disruption of the endoplasmic reticulum. *Mol. Biol. Cell*, **6**, 283–296.
19. Ellenberg, J., Lippincott-Schwartz, J. and Presley, J.F. (1998) Two-color green fluorescent protein time-lapse imaging. *Biotechniques*, **25**, 838–846.
20. Presley, J.F., Cole, N.B., Schroer, T.A., Hirschberg, K., Zaal, K.J. and Lippincott-Schwartz, J. (1997) ER-to-Golgi transport visualized in living cells. *Nature*, **389**, 81–85.
21. Hirschberg, K., Miller, C.M., Ellenberg, J., Presley, J.F., Siggia, E.D., Phair, R.D. and Lippincott-Schwartz, J. (1998) Kinetic analysis of secretory protein traffic and characterization of golgi to plasma membrane transport intermediates in living cells. *J. Cell Biol.*, **143**, 1485–1503.
22. Usami, S., Abe, S., Weston, M.D., Shinkawa, H., Van Camp, G. and Kimberling, W.J. (1999) Non-syndromic hearing loss associated with enlarged vestibular aqueduct is caused by PDS mutations. *Hum. Genet.*, **104**, 188–192.
23. Everett, L.A., Belyantseva, I.A., Noben-Trauth, K., Cantos, R., Chen, A., Thakkar, S.I., Hoogstraten-Miller, S.L., Kachar, B., Wu, D.K. and Green, E.D. (2001) Targeted disruption of mouse *Pds* provides insight about the inner-ear defects encountered in Pendred syndrome. *Hum. Mol. Genet.*, **10**, 153–161.
24. Zeitlin, P.L. (2000) Pharmacologic restoration of delta F508 CFTR-mediated chloride current. *Kidney Int.*, **57**, 832–837.
25. Morello, J.P., Petaja-Repo, U.E., Bichet, D.G. and Bouvier, M. (2000) Pharmacological chaperones: a new twist on receptor folding. *Trends Pharmacol. Sci.*, **21**, 466–469.
26. Taylor, J.P., Metcalfe, R.A., Watson, P.F., Weetman, A.P. and Trembath, R.C. (2002) Mutations of the PDS gene, encoding pendrin, are associated with protein mislocalization and loss of iodide efflux: implications for thyroid dysfunction in Pendred syndrome. *J. Clin. Endocrinol. Metab.*, **87**, 1778–1784.
27. Lippincott-Schwartz, J., Yuan, L., Tipper, C., Amherdt, M., Orci, L. and Klausner, R.D. (1991) Brefeldin A's effects on endosomes, lysosomes, and the TGN suggest a general mechanism for regulating organelle structure and membrane traffic. *Cell*, **67**, 601–615.